Int J Thermophys (2009) 30:167–178
DOI 10.1007/s10765-008-0547-1

Spatial Scatter Effects in the Calibration of IR Pyrometers and Imagers

J. Envall · S. N. Mekhontsev · Y. Zong · L. M. Hanssen

Published online: 10 January 2009

Abstract Differences in the calibration conditions and the real-life applications of infrared pyrometers, radiometers, or imagers can contribute to significant measurement errors due to the presence of scattered light from the areas surrounding the reference source during the calibration process or the measured object in the field measurements. This out-of-field scatter (also known as size-of-source effect, SSE) has to be analyzed separately for each artifact to ensure applicability of the calibration results to the scene of actual measurement. This article discusses SSE characterization methods and specific requirements for calibrating single-element radiometers in the near- and mid-IR parts of the optical radiation spectrum. Two new SSE tools developed at National Institute of Standards and Technology to support routine calibration of IR pyrometers, radiometers, and imagers at the recently developed Advanced Infrared Radiometry and Imaging (AIRI) facility are described. The results of characterization of different commonly used radiometers, including an industrial-grade pyrometer, a high-accuracy pyrometer, two different infrared spectrometers, and an infrared imager, are presented.

Keywords Imager · Infrared (IR) · Pyrometer · Radiometer · Size-of-source effect (SSE) · Spatial scatter

1 Introduction

The spatial scatter effect is a well-known source of measurement error and contributor to uncertainty in radiometric measurements [1–4]. Light outside the field-of-view

J. Envall · S. N. Mekhontsev (✉) · Y. Zong · L. M. Hanssen
Optical Technology Division, National Institute of Standards and Technology,
100 Bureau Drive, Stop 8442, Gaithersburg, MD 20899-8442, USA
e-mail: snm@nist.gov

(FOV) of the measuring instrument causes an unwanted increase in the measured signal. The effect is mainly caused by the scatter of light and aberrations, inter-element reflections, and diffraction in the optical components. This inevitably leads to problems when a radiometer is used to measure the radiance or radiance temperature of targets with variable sizes. Also, the measurement results may be highly erroneous when low-temperature targets are measured against a high-temperature background or if high-temperature objects are placed close to the target. In the case of imagers, this phenomenon is likely to happen for every sensing element (pixel) of the device, which leads to problems such as ghost images [5,6].

Several methods have been introduced to quantify the effect of spatial scatter. If the size of the effect is small, it is often considered a component in the uncertainty budget of the measurement. In some applications, it may be appropriate to calculate a correction to reduce the contribution of the spatial scatter to the measurement results.

For single-element detectors used in measurements of radiance or radiance temperature, the size-of-source effect (SSE) is a useful measure of spatial scatter. It is defined as the ratio of the signal originated from light outside the FOV to the signal for an infinitely large target. In other words, the SSE is a measure of how the physical size of the target affects the measured radiance of the target. Three methods are in common use to measure the SSE: the variable-source method [7], the central obscuration method [8], and the mathematical analysis utilizing the measured point-spread function (PSF) of the detector [9]. For the special case of determining the SSE for a pyrometer measuring a fixed-point blackbody, the blackbody furnace itself, with suitable modifications, can be utilized [10]. When dealing with imagers, the effect of spatial scatter must be taken into account for each pixel.

Most studies of SSE reported so far have concentrated on the visible (0.4 µm to 0.7 µm) and near-infrared (NIR, 0.7 µm to 2 µm) spectral regions. The mid-infrared (MIR, 2 µm to 14 µm) region is especially important in optical thermometry, since the radiation emitted by near-room-temperature objects is concentrated in the MIR. Also, the SSE becomes a significant source of measurement error when targets are measured at temperatures close to the environment temperature, because all the surrounding objects may then be considered sources of stray radiation.

At the Advanced Infrared Radiometry and Imaging (AIRI) facility of the National Institute of Standards and Technology (NIST), we have developed equipment and methods to evaluate the SSE in the NIR and MIR for different types of optical systems, radiometers, and imagers. In this article, we describe these measurement setups and present the results of SSE characterization for several instruments, including IR pyrometers, spectrometers, and imagers, obtained with different measurement methods.

2 SSE Measurements

2.1 Methods

There are three commonly used methods for measuring the SSE of a radiometer. In the variable-source method, the radiometer measures the radiance of a uniform target,

whose diameter can be adjusted with a set of variable apertures. The radiance of the target is measured for different aperture sizes and the value of the SSE, $\sigma(r, r_0)$ is obtained as

$$\sigma(r, r_0) = \frac{S(r) - S(r_0)}{S(\infty)}, \tag{1}$$

where $S(r)$ is the signal measured for the radius r and r_0 is the nominal spot size of the radiometer. In practice, $S(\infty)$ may be replaced with $S(r_{\max})$, where $r_{\max}$ is the maximum aperture radius. In the central obscuration method, the center of the target is blocked with a baffle whose diameter is greater than r_0. When the radiometer is aligned to measure the radiance of the baffle, the signal caused by the surroundings of the baffle, via the SSE, is measured directly. The third option is to measure the PSF of the radiometer. The measured PSF may be utilized to calculate the SSE of the radiometer when the background radiation (simple or complex) is known.

2.2 Comparison of Methods

The three methods, described in Sect. 2.1, were compared in a study conducted at AIRI's sister facility, the Fourier Transform Infrared Spectrophotometric facility for materials characterization [11]. An integrating sphere was used as the radiation source. The diameter of the exit port of the sphere was 37 mm. The output of the sphere was imaged to the fore-optics of the system under test. The nominal spot size of the FOV of the system was set to 3.1 mm. An iris diaphragm was used to restrict the size of the image. The diameter of the iris was varied from 6 mm to 37 mm. The measurement was performed with two wavelengths, 600 nm and 1580 nm. The measurements were repeated using the central obscuration method. A piece of black cloth with a diameter of 6 mm was used as the obscuration. The same wavelengths were used as in the variable-source method measurements. In addition, for the central obscuration method, a third wavelength, 3.7 μm, was used. The radiation source in the latter measurement was a commercial infrared calibrator with a 57 mm flat-plate radiator. The temperature of the plate was set to 500 °C. For detection of the radiation, an InSb radiometer, a chopper, and a lock-in amplifier were used. The distance between the radiator and the object plane was 15 mm. A 6 mm diameter water-cooled blackened target was used as the obscuration at the center of the object plane.

The PSF, or the relative spatial response, of the system was measured with a setup that utilized a point source (a tungsten halogen source covered with a pinhole that was attached to an xy translation stage). A Si filter radiometer was used as the detector. In addition, a monitor detector was used to compensate for the instability and drift of the source. A shutter was used behind the field stop of the system to compensate for the detector offset and stray radiation inside the enclosure of the system. The values of the SSE for different source diameters can be obtained from the measured PSF via integration. The graph of Fig. 1 shows the total flux that reaches the detector as a function of the inner diameter of the circular zone placed in front of the detector, the outer diameter of the zone being fixed to 40 mm. For the system under test in these

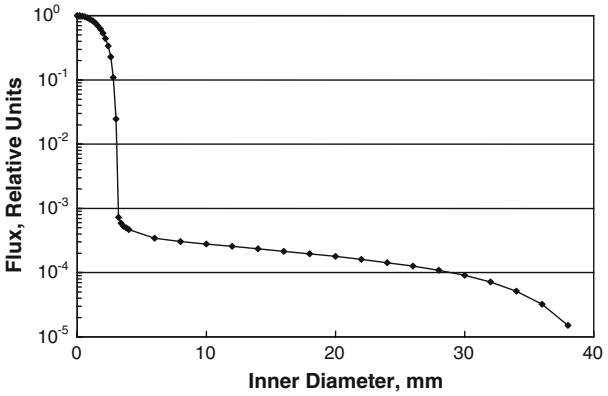

Fig. 1 Total flux reaching the detector as the function of the inner diameter of the circular zone placed in front of the detector, the outer diameter of the zone being fixed to 40 mm. The data were obtained from the measured PSF by integration [11]

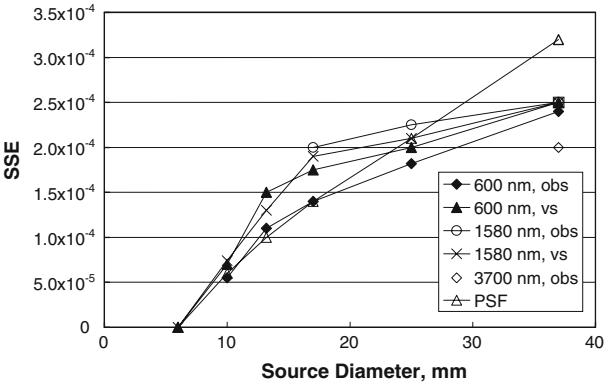

Fig. 2 Comparison of variable-source method (vs), central obscuration method (obs), and the method utilizing the measured PSF. Shown are the measured SSE values for an optical system at three different wavelengths

measurements, the inner diameter was 6 mm. The SSE values were calculated for the diameters used in the measurements with the other two methods.

The results of the comparisons of the three methods of measurement are shown in Fig. 2. The estimated expanded uncertainty ($k = 2$) for the three methods for the data shown in Fig. 2 range from 5×10^{-5} to 1×10^{-4}. It can be seen that the SSE, obtained for the system under test, for source diameters of 6 mm to 25 mm remained below 2.5×10^{-4} for all wavelengths. At 37 mm, the results are consistent with the uncertainties. The somewhat greater value for the integerated PSF data can be associated with the increased uncertainty due to the integration of a small signal over a large area (i.e., accumulation of a small positive offset error). Nevertheless, the absolute value of the SSE was found to be sufficiently low for all methods for the purpose of the facilities measurement requirements.

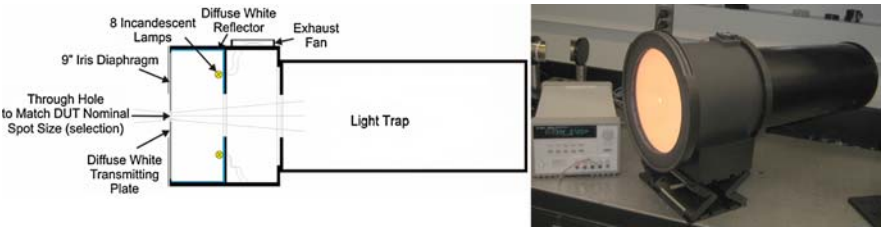

Fig. 3 Structure of SSE1

2.3 AIRI Tools for SSE Measurements

The purpose of the AIRI facility at NIST is to perform accurate and traceable calibrations of radiance temperature and spectral radiance. Specific equipment has been adapted to the facility to enable routine SSE measurements for different types of optical pyrometers, spectrometers, etc., mainly in the IR.

Figure 3 shows a device suitable for SSE measurements with the central obscuration method. This device, named the SSE1, has a diffuse white transmitting plate, behind which there are eight incandescent lamps to illuminate the plate. In the center of the plate there is a through-hole. Several plates with through-holes of different diameters can be used to match the size of the through-hole to the nominal spot size of the radiometer. In front of the transmitting plate there is an iris aperture, whose diameter can be adjusted up to 220 mm. Behind the through-hole there is a large light trap coated with ESLI Vel-Black coating (on the bottom of the trap) and Rippey UltraPol V Cloth [12]. Based on the reflectance properties of the interior surfaces, the cavity was modeled, resulting in an estimated reflectance of the trap less than 3×10^{-5} over the wavelength range from 0.9 µm to 2.5 µm. However, the back surface incurred some minor damage during construction. This resulted in a somewhat greater reflectance and modest increase in signal as seen in the measured results. Nevertheless, the performance is sufficient for the intended purpose of evaluation of devices used to view large-area sources.

The SSE1 was used to measure the SSE of a high-accuracy pyrometer, the RT1550, used as a transfer standard for radiance temperature. The operating wavelength of the pyrometer is 1550 nm. A further description of the pyrometer is given in [13]. The measurements were performed with aperture sizes ranging from 12.6 mm to 37 mm. The SSE was measured with a second device of the AIRI facility, named the SSE2. The structure of SSE2 is described in an earlier publication [14]. The measured SSE values, obtained with both devices, are shown in Fig. 4. The measured SSE for the pyrometer was 5×10^{-5} for the maximum aperture diameter of 37 mm. This value would correspond to a 10 mK temperature change when measuring at the gold fixed-point temperature of 1064 °C. The data shown in Fig. 4 demonstrate a difference in the measured SSE for the two devices, SSE1 and SSE2. The higher values measured with SSE1 are likely caused by the non-ideal absorbing cavity used in the device, as discussed above. The structure of SSE2 more effectively rejects back reflections from the cavity. However, the relatively low value of this additional signal is not a limiting factor in routine calibrations for customer devices.

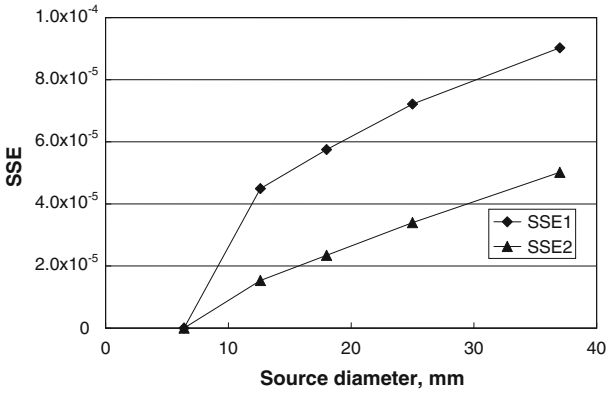

Fig. 4 SSE of pyrometer RT1550, measured with SSE1 and SSE2

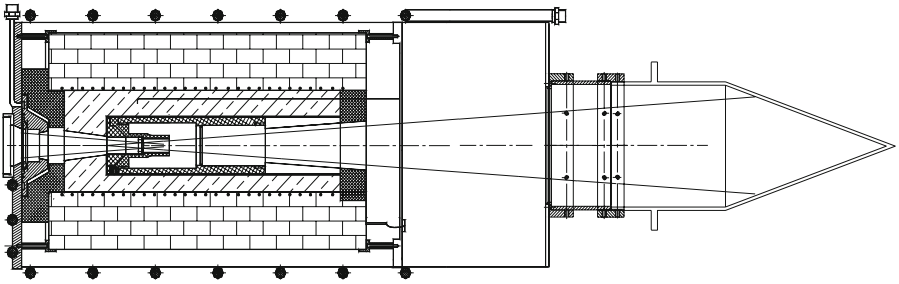

Fig. 5 Schematic of the measurement setup when utilizing a blackbody furnace in the SSE measurements. The crucible has been replaced with an empty one with the rear half removed. A light trap has been added to the rear of the blackbody

In the AIRI facility, fixed-point blackbody sources are used as reference sources for radiance temperature when calibrating pyrometers. The SSE arising from a blackbody greatly depends on the shape of the structure of the blackbody. Therefore, in order to evaluate the SSE in pyrometer calibrations accurately, it may not be sufficient to measure the SSE of the pyrometer with the equipment and techniques described above. Therefore we decided to apply the method described by Jones and Tapping [10]. In this method, the blackbody furnace itself is used in the measurement of the SSE, as seen in Fig. 5. The crucible, normally containing metal to be melted, is replaced with an empty one. The rear half of the crucible is removed and an absorbing cone is attached to the rear flange of the furnace, filling the ideal FOV of the pyrometer. Figure 6 shows the results of this measurement performed on a high-accuracy pyrometer, named the RT900, operating at 900 nm. Also shown for comparison is the SSE measured utilizing the SSE2.

Figure 7 shows the structure of the device we use to measure the SSE in the MIR region. The device, named the SSEIR, has a heated emitter plate. In the center of the plate, there is a through-hole, behind which there is a blackbody at the same temperature as the emitter plate. The size of the portion of the emitter plate, visible to the radiometer under test, can be set by placing different reflecting shields with apertures

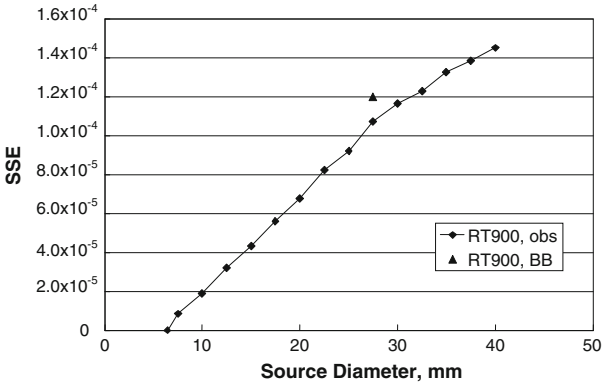

Fig. 6 SSE of pyrometer RT900, obtained with the central obscuration method (obs) and the method utilizing the blackbody furnace (BB)

of variable sizes in front of the emitter plate. The reflecting shield is meant to be at ambient temperature. In order to test the dependence of the shield temperature on the temperature of the emitter plate, two scans were made. Figure 8 shows the results of these scans as the spatial dependence of the measured radiance temperature. In both scans, the temperature of the blackbody was kept at 49 °C. The shield temperature is seen to be fairly independent of the temperature of the emitter plate. The temperature of the emitter plate was set to 15 °C and 50 °C, respectively. The ambient air temperature was approximately 25 °C. Figure 9 shows the measured SSE, using the SSEIR, for an industrial pyrometer (8 µm to 14 µm). Shown on the right side is the temperature error corresponding to the SSE. The measurements were performed for a source at 70 °C and the results are given relative to an aperture of 12.7 mm diameter. The results obtained for the pyrometer show that, for a target at 70 °C, the SSE may cause an error of several degrees in the measured temperature with large target sizes. Figure 10 shows the measured SSE of a NIST spectral comparator. The measurement wavelength was 3.7 µm. The results obtained for the NIST spectral comparator indicated excellent performance, and the SSE values were found negligible for most measurement situations.

3 Spatial Scatter with Imagers

The spatial scatter inside imagers is a phenomenon that has been under some increasing focus during recent years [15,16]. This is a natural consequence of the application of imagers to many fields, including astronomy, remote sensing, optical thermometry, and various military applications. The issue of spatial scatter inside an imager is similar to that of spatial scatter inside a single-element detector, with the exception that, when dealing with an imager, the scattered radiation is present on all the pixels of the device. Spatial scatter in an imager can cause ghost images. The causes of spatial scatter in imagers are the same as those in single-element detectors, except that images may have additional "spatial scatter" caused by the electronic crosstalk

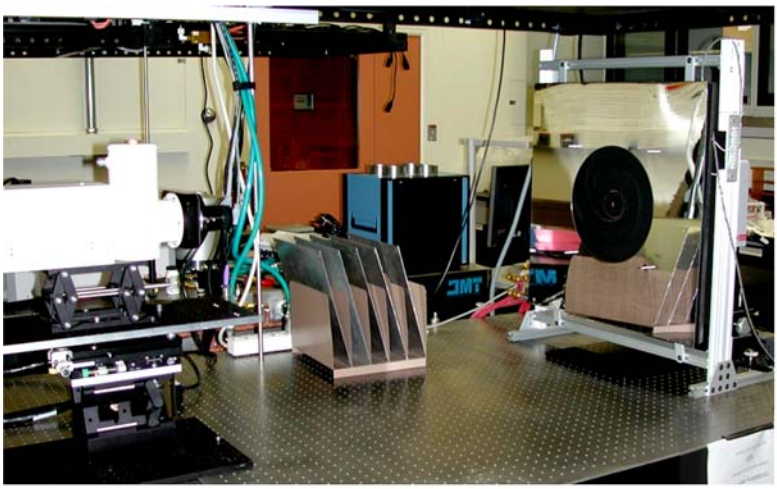

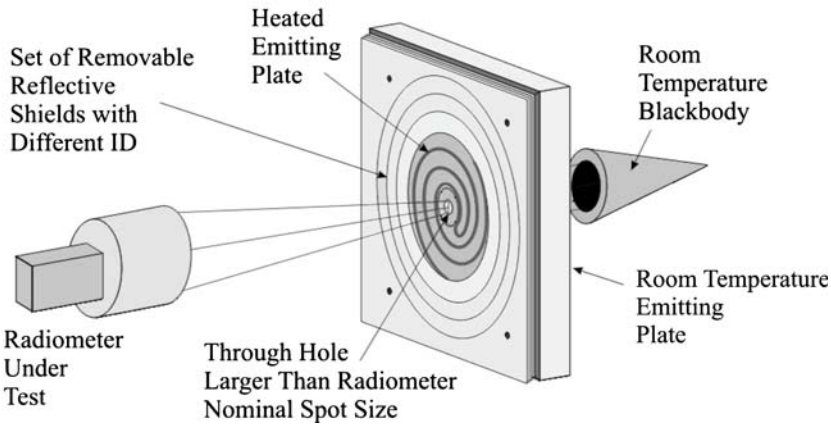

Fig. 7 Structure of SSEIR

between pixels. In radiometric applications where the absolute value of the signal of each pixel is of interest, spatial scatter causes measurement error to each value. In absolute radiance temperature measurements, especially with near-ambient temperatures, significant errors may occur due to the large impact of background radiation on the measured results.

3.1 Figures of Merit

Several figures of merit have been introduced to validate the quality of imagers with regard to their performance in the presence of stray radiation. These include ensquared power (EP), aperiodic transfer function (ATF), and slit response function (SRF). The EP is defined as the ratio of the signal of the central pixel of the imager to the summed

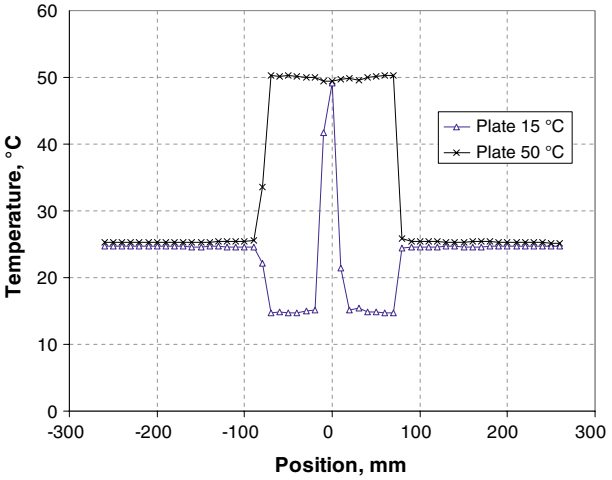

Fig. 8 Horizontal scan showing the spatial dependence of the radiance temperature of the MIR SSE device. Flat regions of the curve at ∼ 25 °C represent the temperature of the reflecting shield that is close to the ambient air temperature. The temperature measured at the center is the temperature of the blackbody that is set to 49 °C. The temperature of the emitter plate was set to 15 °C and 50 °C during the two scans

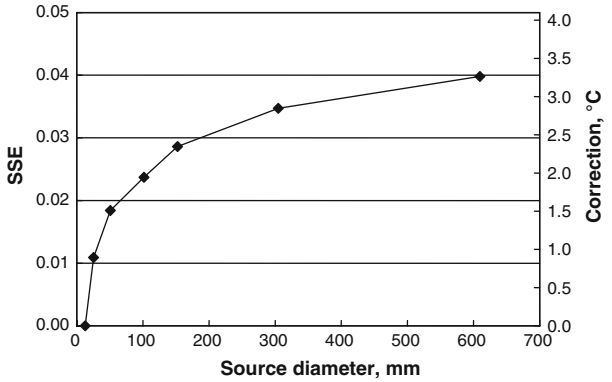

Fig. 9 Measured SSE for an industrial pyrometer. The temperature of the source was 70 °C, and the results are given relative to a 13 mm aperture. Also, the temperature corrections for this source are given

signals of all pixels, when the imager is viewing a point source. The ATF of the system describes how the signal of a pixel changes as a function of source area, when the source intensity is kept constant. The maximum value of the ATF is normalized to unity. For an ideal detector, when the source area is smaller than the projected area of the detector, the ATF increases linearly when the source area is increased; when the source area exceeds the projected detector area, the value of the ATF, remains at unity. For practical imagers, the values of the ATF remain below the ideal function shape, approaching it as the source area is increased. The definition of the SRF is quite close to that of the ATF, with the exception that instead of the source area the angular subtendence of the source is used as the variable. Two important figures of

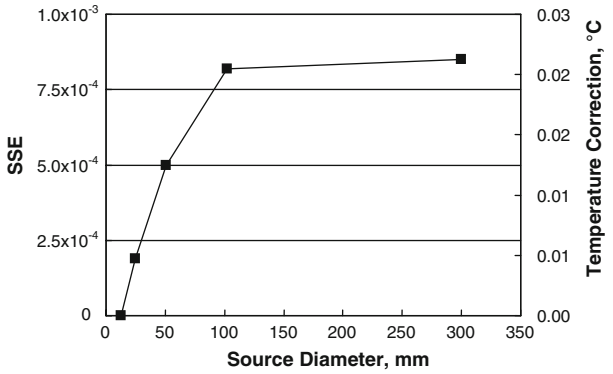

Fig. 10 Measured SSE for a NIST spectral comparator. The measurement wavelength was 3.7 µm. The temperature corrections are also given

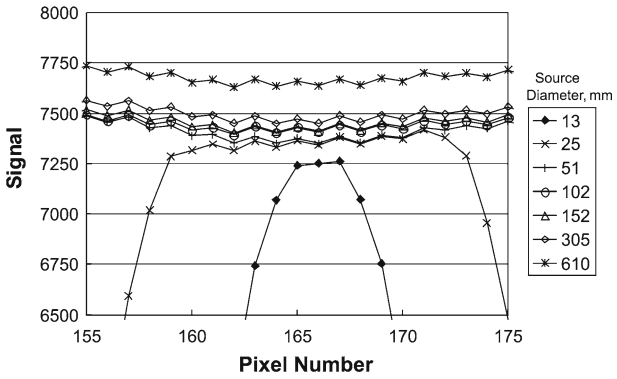

Fig. 11 Measured signal of each pixel of a commercial IR imager for seven different source diameters

merit can be determined from the SRF; these are the imaging resolution (in radians) and the measurement resolution. They are defined as the angles for which the SRF has the values 0.5 and 0.99, respectively. The measurement resolution is an important figure in radiometry, since it determines approximately the minimum source size for which the measured radiance is reproducible.

3.2 Experimental Measurement of Spatial Scatter of a Commercial Imager

The spatial scatter characteristics of a commercial imager were studied with the SSEIR device. Figure 11 shows the signal of individual pixels as a function of pixel number for seven different source sizes. The temperature of the source was 50 °C, while the background was kept at 23 °C. As can be seen, the signal on the center pixels increases when the source size is increased. This gives a qualitative demonstration of the presence of stray radiation. Figure 12 shows the temperature correction that needs to be applied to compensate for the spatial scatter effect for this measurement situation, as a function of source diameter.

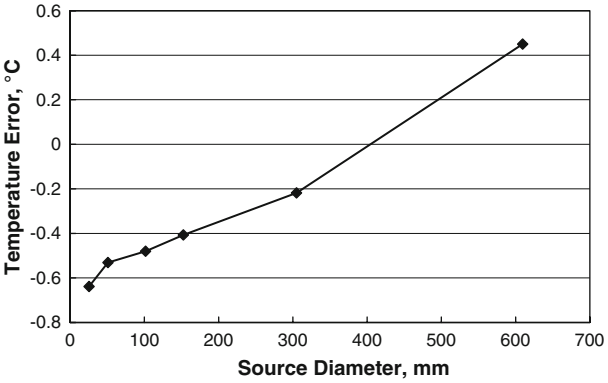

Fig. 12 Temperature error to be subtracted from the measured value to compensate for the spatial scatter effect of a commercial IR imager

A simple matrix method for correcting errors resulting from spatial scatter has been developed [16], and will be used to correct the imager for spatial scatter errors. This method is based on the characterization of an imager for a set of PSF. By using the measured PSFs, a spatial scatter correction matrix is derived and the correction is simply a matrix multiplication of correction matrix and the measured raw image. By using this method, the spatial scatter errors can be reduced by more than one order of magnitude. The details of the correction and results will be presented in a future publication.

4 Discussion and Conclusions

Three methods to measure the SSE of an optical system, the variable source method, the central obscuration method, and the method utilizing the measured PSF, were compared. The results obtained for the system under test showed reasonable agreement between all three methods, considering the levels of uncertainty. Several instruments were developed for the purpose of SSE measurements at the AIRI facility of NIST. We demonstrated a very low level of the SSE for a pyrometer operating at 1550 nm. We also demonstrated agreement between a direct measurement of the SSE using an actual heated, modified fixed-point blackbody source and our SSE2 test device, with a pyrometer operating at 900 nm. The new instruments developed also include a setup, named the SSEIR, that enables measurements in the thermal infrared wavelength region and is designed to take into account the effects of the ambient background on a source characterization. Several devices were characterized using the SSEIR, including an industrial pyrometer and a NIST spectral comparator, with the corresponding measured SSE ranging from several percent to less than 0.1 %, respectively.

Spatial scatter inside IR imagers was briefly discussed. Significant errors in a measured raw image were demonstrated by using a commercial imager and the SSEIR instrument.

References

1. M. Ohtsuka, R.E. Bedford, Measurement **7**, 2 (1989)
2. P. Bloembergen, in *Proceedings of TEMPMEKO '99, 7th International Symposium on Temperature and Thermal Measurements in Industry and Science*, ed. by J.F. Dubbeldam, M.J. de Groot (Edauw Johannissen bv, Delft, 1999), pp. 607–612
3. P. Marcarino, T. Ricolfi, Metrologia **33**, 291 (1996)
4. H.W. Yoon, D.W. Allen, R.D. Saunders, Metrologia **42**, 89 (2005)
5. P. Saunders, H. Edgar, High Temp. High Press. **31**, 283 (1999)
6. H. Tonooka, IEEE Trans. Geosci. Remote Sens. **43**, 2752 (2005)
7. T.J. Quinn, T.R.D. Chandler, in *Temperature, Its Measurement and Control in Science and Industry*, vol. 4, part 1, ed. by H. Plumb (ISA, Pittsburgh, 1972), pp. 295–309
8. P.B. Coates, J.W. Andrews, J. Phys. F: Met. Phys. **8**, 277 (1978)
9. B.C. Johnson, J.B. Fowler, C.L. Cromer, in *The SeaWiFS Transfer Radiometer (SXR)*, NASA Tech. Memo 1998–206892, vol. 1, ed. by S.B. Hooker, E.R. Firestone (NASA Goddard Space Flight Center, Greenbelt, MD, 1998), p. 58
10. T.P. Jones, J. Tapping, Metrologia **18**, 23 (1982)
11. S. Mekhontsev, L. Hanssen, in *Temperature: Its Measurement and Control in Science and Industry*, vol. 7, part 1, ed. by D.C. Ripple (AIP, New York, 2003), pp. 693–698
12. Certain commercial equipment, instruments, or materials are identified in this paper for information only. Such identification does not imply recommendation or endorsement by the National Institute of Standards and Technology
13. M. Noorma, S. Mekhontsev, V. Kromchenko, A. Gura, M. Litorja, B. Tsai, L. Hanssen, Proc. SPIE **6205**, 620501 (2006)
14. S. Mekhontsev, V. Khromchenko, A. Prokhorov, L. Hanssen, in *Proceedings of TEMPMEKO 2004, 9th International Symposium on Temperature and Thermal Measurements in Industry and Science*, ed. by D. Zvizdic (FSB/LPM, Zagreb, Croatia, 2004), pp. 581–586
15. D. Hong, K.J. Voss, Appl. Optics **43**, 665 (2004)
16. Y. Zong, S.W. Brown, K.R. Lykke, Y. Ohno, in *Proceedings of the 26th Session of the CIE*, Beijing (2007)